crystallization. The sequence of the oligonucleotide that yielded cocrystals is 5′-CGCAACT↓T-3′ where ↓ denotes the preferred site of cleavage. The binding affinity of TopoIII-Y328F for this oligonucleotide was measured by fluorescence polarization with 5′-fluorescein-labelled DNA. Reactions were prepared in 50 mM Tris (pH 8.0) and 100 mM NaCl, and allowed to equilibrate for 3 min at 25 °C before taking polarization measurements.

The complex was prepared for crystallization by incubating TopoIII-Y328F (4 mg ml^{-1}) with a twofold molar excess of oligonucleotide at 4 °C for 30 min. Cocrystals formed at 22 °C in hanging drops equilibrated against 1.3 M $(NH_4)_2SO_4$, 0.1 M sodium citrate (pH 5.5), and 0.8 M NaCl. Crystals appeared in 2–3 d and grew as thin plates to maximum dimensions of ~0.05 × 0.2 × 1 mm^3 within 2 weeks. The crystals belong to space group C2 with cell dimensions of a = 122.0 Å, b = 60.8 Å, c = 125.4 Å, and β = 90.7°, and contain one complex per asymmetric unit. Before data collection, the crystals were quickly transferred in a single step to mother liquor supplemented with 25% glycerol and flash-cooled in liquid nitrogen. For the magnesium studies, crystals were soaked for 16 h in mother liquor containing 10 mM $MgCl_2$ before transfer to the cryoprotectant containing 10 mM $MgCl_2$. Macromolecular crystal annealing was performed to decrease crystal mosaicity[22]. Crystals diffracted to 2.0 Å at 100 K with synchrotron radiation, although they still displayed a large mosaicity (>1.5°). Diffraction data were collected in 0.5° oscillation steps due to the large mosaicity, processed with the program XDS[23], and scaled with SCALA[24]. Data collection statistics are available (see Table I in Supplementary Information).

Structure determination and refinement

The structure of the complex was solved by molecular replacement with AMORE[24] using diffraction data from a single crystal. The initial search model consisted of domains I and IV (residues 1–216; 489–609) from the 3.0 Å resolution structure of *E. coli* DNA topoisomerase III[3]. Rotation and translation searches performed with data to 3 Å yielded a clear solution for this region of the protein. Domains I and IV were then fixed, and a solution for domains II and III together was found that gave an *R*-factor of 49.8% for the entire model. Initial refinement was carried out to 3 Å, and consisted of rigid body refinement of the individual domains interspersed with cycles of simulated annealing and conjugate gradient minimization in CNS[25]. The resolution was gradually extended to 2.05 Å as the *R*-factor decreased. Initial electron-density maps were improved by density modification in CNS, and showed unambiguous density for all eight bases of the oligonucleotide. Building of the DNA model and rebuilding of the protein model was carried out in program O[26], and all refinement was done in CNS. A large region of domain IV had undergone rearrangements and needed to be rebuilt. Density could be seen for a short surface loop (185–190) and additional C-terminal residues that were disordered in the apo topoisomerase III structure. A strong difference density peak (>8σ) present near the 5′ end of the oligonucleotide was assigned as a chloride ion. The structure was refined to an *R* factor of 23.3% and an R_{free} of 26.0%, with 90.5% of all residues in the most favoured regions of the Ramachandran plot and no residues in the disallowed regions. The final model contains residues 1–620 of TopoIII-Y328F, the entire oligonucleotide, 332 water molecules, one sulphate molecule, and one chloride ion. Refinement statistics are available (see Table I in Supplementary Information). Figures were made with the programs GRASP[27], MOLSCRIPT[28], RASTER3D[29] and SETOR[30].

Received 4 January; accepted 2 May 2001.

1. Wang, J. C. DNA topoisomerases. *Annu. Rev. Biochem.* **65,** 635–692 (1996).
2. Zhang, H. L., Malpure, S. & DiGate, R. J. *Escherichia coli* DNA topoisomerase III is a site-specific DNA binding protein that binds asymmetrically to its cleavage site. *J. Biol. Chem.* **270,** 23700–23705 (1995).
3. Mondragon, A. & DiGate, R. The structure of *Escherichia coli* DNA topoisomerase III. *Struct. Fold Des.* **7,** 1373–1383 (1999).
4. Zhang, H. L. & DiGate, R. J. The carboxyl-terminal residues of *Escherichia coli* DNA topoisomerase III are involved in substrate binding. *J. Biol. Chem.* **269,** 9052–9059 (1994).
5. Li, Z., Mondragon, A., Hiasa, H., Marians, K. J. & DiGate, R. J. Identification of a unique domain essential for *Escherichia coli* DNA topoisomerase III-catalysed decatenation of replication intermediates. *Mol. Microbiol.* **35,** 888–895 (2000).
6. Lima, C. D., Wang, J. C. & Mondragon, A. Three-dimensional structure of the 67K N-terminal fragment of *E. coli* DNA topoisomerase I. *Nature* **367,** 138–146 (1994).
7. Sherratt, D. J. & Wigley, D. B. Conserved themes but novel activities in recombinases and topoisomerases. *Cell* **93,** 149–152 (1998).
8. Redinbo, M. R., Champoux, J. J. & Hol, W. G. Novel insights into catalytic mechanism from a crystal structure of human topoisomerase I in complex with DNA. *Biochemistry* **39,** 6832–6840 (2000).
9. Chen, S. J. & Wang, J. C. Identification of active site residues in *Escherichia coli* DNA topoisomerase I. *J. Biol. Chem.* **273,** 6050–6056 (1998).
10. Zhu, C. X., Roche, C. J., Papanicolaou, N., DiPietrantonio, A. & Tse-Dinh, Y. C. Site-directed mutagenesis of conserved aspartates, glutamates and arginines in the active site region of *Escherichia coli* DNA topoisomerase I. *J. Biol. Chem.* **273,** 8783–8789 (1998).
11. Wang, J. C. Interaction between DNA and an *Escherichia coli* protein ω. *J. Mol. Biol.* **55,** 523–533 (1971).
12. Domanico, P. L. & Tse-Dinh, Y. C. Mechanistic studies on *Escherichia coli* DNA topoisomerase I: Divalent ion effects. *J. Inorg. Biochem.* **42,** 87–96 (1991).
13. Zhu, C. X. & Tse-Dinh, Y. C. The acidic triad conserved in type IA DNA topoisomerases is required for binding of Mg(II) and subsequent conformational change. *J. Biol. Chem.* **275,** 5318–5322 (2000).
14. Nichols, M. D., DeAngelis, K., Keck, J. L. & Berger, J. M. Structure and function of an archaeal topoisomerase VI subunit with homology to the meiotic recombination factor Spo11. *EMBO J.* **18,** 6177–6188 (1999).
15. Berger, J. M., Fass, D., Wang, J. C. & Harrison, S. C. Structural similarities between topoisomerases that cleave one or both DNA strands. *Proc. Natl Acad. Sci. USA* **95,** 7876–7881 (1998).
16. Aravind, L., Leipe, D. D. & Koonin, E. V. Toprim-a conserved catalytic domain in type IA and II topoisomerases, DnaG-type primases, OLD family nucleases and RecR proteins. *Nucleic Acids Res.* **26,** 4205–4213 (1998).
17. Keck, J. L., Roche, D. D., Lynch, A. S. & Berger, J. M. Structure of the RNA polymerase domain of *E. coli* primase. *Science* **287,** 2482–2486 (2000).
18. Podobnik, M., McInerney, P., O'Donnell, M. & Kuriyan, J. A TOPRIM domain in the crystal structure of the catalytic core of *Escherichia coli* primase confirms a structural link to DNA topoisomerases. *J. Mol. Biol.* **300,** 353–362 (2000).
19. Liu, Q. & Wang, J. C. Similarity in the catalysis of DNA breakage and rejoining by type IA and IIA DNA topoisomerases. *Proc. Natl Acad. Sci. USA* **96,** 881–886 (1999).
20. Berger, J. M., Gamblin, S. J., Harrison, S. C. & Wang, J. C. Structure and mechanism of DNA topoisomerase II. *Nature* **379,** 255–232 (1996).
21. Fass, D., Bogden, C. E. & Berger, J. M. Quaternary changes in topoisomerase II may direct orthogonal movement of two DNA strands. *Nature Struct. Biol.* **6,** 322–326 (1999).
22. Harp, J. M., Timm, D. E. & Bunick, G. J. Macromolecular crystal annealing: overcoming increased mosaicity associated with cryocrystallography. *Acta Crystallogr. D* **54,** 622–628 (1998).
23. Kabsch, W. Automatic processing of rotation diffraction data from crystals of initially unknown symmetry and cell constants. *J. Appl. Crystallogr.* **26,** 795–800 (1993).
24. Collaborative Computational Project 4. The CCP4 suite: programs for protein crystallography. *Acta Crystallogr. D* **50,** 760–763 (1994).
25. Brunger, A. T. *et al.* Crystallography & NMR system: A new software suite for macromolecular structure determination. *Acta Crystallogr. D* **54,** 905–921 (1998).
26. Jones, T. A., Zou, J. Y., Cowan, S. W. & Kjeldgaard, M. Improved methods for building protein models in electron density maps and the location of errors in these models. *Acta Crystallogr. A* **47,** 110–119 (1991).
27. Nicholls, A., Sharp, K. A. & Honig, B. H. Protein folding and association: insights from the interfacial and thermodynamic properties of hydrocarbons. *Proteins Struct. Funct. Genet.* **11,** 281–286 (1991).
28. Kraulis, P. J. MOLSCRIPT: a program to produce both detailed and schematic plots of protein structures. *J. Appl. Crystallogr.* **24,** 946–950 (1991).
29. Merritt, E. A. & Murphy, M. E. P. Raster 3D version 2.0. A program for photorealistic molecular graphics. *Acta Crystallogr. D* **50,** 869–873 (1994).
30. Evans, S. V. SETOR: Hardward lighted three-dimensional solid model representations of macromolecules. *J. Mol. Graphics* **11,** 134–138 (1993).

Supplementary information is available on *Nature*'s World-Wide Web site (http://www.nature.com) or as paper copy from the London editorial office of *Nature*.

Acknowledgements

We acknowledge the contributions of H. Feinberg to the early stages of this project, and thank W. Niu for technical assistance. We thank K. Perry, E. Sontheimer and J. Widom for comments and suggestions. Research was supported by the NIH (A.M.) and an NRSA Institutional Training Grant in Molecular Biophysics (A.C.). We acknowledge the use of instruments in the Keck Biophysics Facility at Northwestern University. Portions of this work were performed at the DuPont-Northwestern-Dow collaborative Access Team (DND-CAT) Synchrotron Research Center at the Advanced Photon Source and at the Stanford Synchrotron Radiation Laboratory (SSRL). DND-CAT is supported by DuPont, Dow and the NSF, and use of the APS is supported by the DOE. SSRL is operated by the DOE, Office of Basic Energy Sciences. The SSRL Biotechnology Program is supported by the NIH and the DOE.

Correspondence and requests for materials should be addressed to A.M. (e-mail: a-mondragon@northwestern.edu). Coordinates have been deposited in the Protein Data Bank under the accession code 117D.

correction

A conserved XIAP-interaction motif in caspase-9 and Smac/DIABLO regulates caspase activity and apoptosis

Srinivasa M. Srinivasula, Ramesh Hegde, Ayman Saleh, Pinaki Datta, Eric Shiozaki, Jijie Chai, Ryung-Ah Lee, Paul D. Robbins, Teresa Fernandes-Alnemri, Yigong Shi & Emad S. Alnemri

Nature **410,** 112–116 (2001).

It has been brought to our attention by Paul Robbins (University of Pittsburgh) that the wrong western blot may have been used by Ayman Saleh in his laboratory to generate the Casp-9 (WT) control panel (second panel from the top) of Fig. 2b. However, we have repeated the experiment and the results and conclusions are unchanged. □

A conserved XIAP-interaction motif in caspase-9 and Smac/DIABLO regulates caspase activity and apoptosis

Srinivasa M. Srinivasula*, Ramesh Hegde*, Ayman Saleh†, Pinaki Datta*, Eric Shiozaki‡, Jijie Chai‡, Ryung-Ah Lee*, Paul D. Robbins†, Teresa Fernandes-Alnemri*, Yigong Shi‡ & Emad S. Alnemri*

** Center for Apoptosis Research and the Department of Microbiology and Immunology, Kimmel Cancer Institute, Thomas Jefferson University, Philadelphia, Pennsylvania 19107, USA*
† Department of Molecular Genetics and Biochemistry, University of Pittsburgh, Pittsburgh, Pennsylvania 15261, USA
‡ Department of Molecular Biology, Lewis Thomas Laboratory, Princeton University, Princeton, New Jersey 08544, USA

X-linked inhibitor-of-apoptosis protein (XIAP) interacts with caspase-9 and inhibits its activity[1–3], whereas Smac (also known as DIABLO) relieves this inhibition through interaction with XIAP[4–7]. Here we show that XIAP associates with the active caspase-9–Apaf-1 holoenzyme complex through binding to the amino terminus of the linker peptide on the small subunit of caspase-9, which becomes exposed after proteolytic processing of procaspase-9 at Asp 315. Supporting this observation, point mutations that abrogate the proteolytic processing but not the catalytic activity of caspase-9, or deletion of the linker peptide, prevented caspase-9 association with XIAP and its concomitant inhibition. We note that the N-terminal four residues of caspase-9 linker peptide share significant homology with the N-terminal tetra-peptide in mature Smac and in the *Drosophila* proteins Hid/Grim/Reaper[8,9], defining a conserved class of IAP-binding motifs. Consistent with this finding, binding of the caspase-9 linker peptide and Smac to the BIR3 domain of XIAP is mutually exclusive, suggesting that Smac potentiates caspase-9 activity by disrupting the interaction of the linker peptide of caspase-9 with BIR3. Our studies reveal a mechanism in which binding to the BIR3 domain by two conserved peptides, one from Smac and the other one from caspase-9, has opposing effects on caspase activity and apoptosis.

Recent data suggest that processing of procaspase-9 might be required for inhibition by XIAP[3], as the overexpression of XIAP was not able to inhibit DNA damage-induced processing of procaspase-9 in U-937 cells, but inhibited the catalytic activity of processed caspase-9. To understand the mechanism of inhibition of the caspase-9–Apaf-1 holoenzyme complex, we decided to reconstitute *in vitro* caspase-9–Apaf-1 holoenzyme complexes containing either fully processed caspase-9 or unprocessed procaspase-9 and study their interaction with—and inhibition by—XIAP. To produce fully processed caspase-9 we overexpressed wild-type (WT) procaspase-9 in bacteria, which resulted in complete processing of procaspase-9 into its p35 and p12 subunits (Fig. 1b, lane 2). Sequence analysis of the purified recombinant caspase-9 revealed that >90% of caspase-9 processing in bacteria occurs at Asp 315, which generates the p35 and p12 subunits, and the remaining 10% of processing occurs at Asp 330 to generate the p10 subunit. Minor processing was also detected at Glu 306. To produce a recombinant unprocessed procaspase-9 it was necessary to mutate Asp 315, Asp 330 and Glu 306 to Ala (Fig. 1a). Overexpression of the triple-mutant procaspase-9 (E306/D315/D330A) produced an unprocessed protein (Fig. 1b, lane 3). When the processed WT caspase-9 or the triple-mutant procaspase-9 proteins were reconstituted with purified Apaf-1 at physiological concentrations (20 nM each), the triple-mutant procaspase-9 was as efficient as the fully processed WT caspase-9 in processing procaspase-3 C163A (Fig. 1c). The triple mutant was also as efficient as the fully processed WT caspase-9 in inducing DEVD-AMC (Asp-Glu-Val-Asp-7-amino-4-methyl coumarin) cleavage in Apaf-1–caspase-9-deficient S100 fraction in the presence of Apaf-1, cytochrome *c*, and dATP, but not in their absence (Fig. 1d).

Given that both processed and unprocessed caspase-9–Apaf-1 holoenzyme complexes are catalytically active, we asked whether XIAP could inhibit them equally. As shown in Fig. 2a, XIAP did not significantly inhibit the processing of procaspase-3 by the holoenzyme that contains the mutant caspase-9 but completely inhibited the processing by the holoenzyme that contains the WT caspase-9. The loss of inhibition of the catalytic activity of the holoenzyme containing the mutant caspase-9 could be due to the inability of XIAP to associate with the uncleavable caspase-9 in the holoenzyme complex. To test this hypothesis, we analysed the two complexes after incubation with XIAP, using gel filtration on a Superose-6 fast protein liquid chromatography (FPLC) column. As shown in Fig. 2b, both WT and uncleavable caspase-9 can form large (molecular mass, 1.4×10^3 KDa) holoenzyme complexes with Apaf-1 after stimulation with cytochrome *c* and dATP. We note that XIAP co-migrated with the WT caspase-9–Apaf-1 complex but not with the uncleavable caspase-9–Apaf-1 complex (Fig. 2b). Activity assays on the peak fractions containing the holoenzymes revealed that the

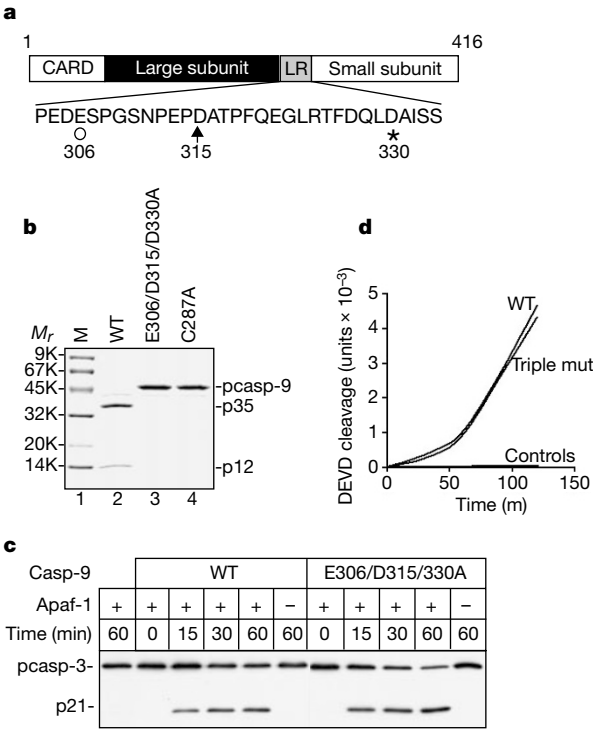

Figure 1 Proteolytic processing of procaspase-9 is not required for activation by Apaf-1. **a**, Bar diagram representing human procaspase-9 and the positions of the autocatalytic cleavage site (Asp 315, arrow) and caspase-3 cleavage site (Asp 330, star) within the linker region (LR) between the large and small subunits. The position of the minor autocatalytic cleavage site (Glu 306, circle) is also shown. **b**, Coomassie stained gel of recombinant WT (lane 2), triple-mutant E306/D315/D330A (lane 3) and active site mutant C287A caspase-9 (lane 4) purified on Talon-affinity resin from bacterial extracts. Lane 1, molecular-mass marker. **c**, Time course analysis of processing of procaspase-3 by the WT and triple-mutant caspase-9 holoenzyme complexes determined by western blotting. **d**, Time course analysis of the DEVD-AMC cleaving activity of caspase-9–Apaf-1-deficient S100 extracts reconstituted with Apaf-1 and WT or triple-mutant caspase-9 proteins. Controls represent WT and triple-mutant caspase-9 proteins incubated with the S100 extracts plus Apaf-1 without cytochrome *c* and dATP.

uncleavable complex was able to process procaspase-3 (Fig. 2c, lane II), whereas the WT complex was completely inactive (lane I). A control WT caspase-9–Apaf-1 complex that was reconstituted without XIAP was fully active (lane III). This shows that XIAP can associate with, and inhibit the activity of, the WT-caspase-9–Apaf-1 complex, but not the uncleavable caspase-9–Apaf-1 complex, suggesting that processing of caspase-9 at the interdomain linker region is important for binding to XIAP. To further confirm the gel filtration data, we incubated XIAP with purified WT or uncleavable caspase-9-holoenzyme complexes and then immunoprecipitated the complexes with an anti Apaf-1 antibody. Only the WT caspase-9–Apaf-1 complex contained XIAP (Fig. 2d, upper panel). These data are consistent with recent observations which revealed that XIAP does not inhibit activation of procaspase-9 but inhibits the activity of the processed caspase-9 in cells undergoing apoptosis[3].

Because the uncleavable caspase-9–Apaf-1 complex is catalytically active, the inability of XIAP to associate with it and inhibit its activity suggests that the association between caspase-9 and XIAP does not require the active site cysteine, but probably involves residues exposed after autoprocessing of procaspase-9 at Asp315. Examination of the free N-terminus of the human, mouse and *Xenopus* p12 subunit of caspase-9, generated after autoprocessing at Asp 315[10], revealed that they all contain a 4-residue motif similar to the BIR3-interaction motif present at the N-terminus of mature Smac (Fig. 3a). This motif also has significant homology to the IAP-interaction motif at the N-termini of the *Drosophila* proteins Hid, Reaper and Grim[8,9] (Fig. 3a). To determine whether this conserved motif interacts with XIAP, we performed *in vitro* interaction assays with ^{35}S-labelled full-length XIAP, or isolated BIR3 domain of XIAP and GST fusion proteins of p12, p10 or the linker peptide (Fig. 3b). Both p12 and the linker peptide were able to interact with full-length XIAP as well as the isolated BIR3 domain of XIAP. However, the p10-GST fusion protein was able to interact only weakly (~50 to 100 times less) with the full-length XIAP or the BIR3 domain. This weak interaction is due to the conservation of the first two residues of the BIR3-binding motif on the N-terminus of p10 (human, Ala331-Ile332; mouse, Ala331-Val332). Single point mutation of these two residues completely abolished the weak interaction between XIAP/BIR3 and p10 (data not shown). As the BIR3 domain of XIAP is the domain that specifically targets caspase-9[1], this suggests that the interaction between the linker peptide of caspase-9 and the BIR3 domain is primarily responsible for this inhibition. The above results were further confirmed using far-western blot analysis with ^{35}S-labelled XIAP. XIAP was able to bind to the WT p12 subunit of caspase-9, p12-GST and Smac-GST bands, but not to variants of caspase-9 with Asp 315 to Ala mutation or p10-GST bands on the nitrocellulose filter (Fig. 3c). The absence of interaction between p10 and XIAP by far western suggests that the observed weak interaction (Fig. 3b) is not physiologically significant. These results indicate that cleavage of caspase-9 at Asp 315 exposes the XIAP-binding motif in the linker region allowing binding to the BIR3 domain of XIAP and concomitant inhibition of caspase-9 activity.

To determine the importance of the linker peptide for inhibition of caspase-9, we deleted residues 316–330 from caspase-9 and expressed it in bacteria. This mutant (with a deleted linker: 'Δlinker') was able to undergo complete processing to generate the p35 and p10 subunits (Fig. 3d, left panel). As expected, the deletion mutant significantly lost the ability to interact with and to be inhibited by BIR3 (Fig. 3d, middle and right panels). This confirms that the p10 subunit of caspase-9 is not the primary target of XIAP-inhibition, and that the linker peptide is required for binding to BIR3 and for inhibition of caspase-9 activity.

To determine the importance of the first two residues of caspase-9-p12, we mutated them to SG or GG. The AT/SG or AT/GG mutants were completely processed at Asp 315 to generate the p35 and p12 subunits (Fig. 3d, left panel, lanes SG and GG). Like the linker-deletion mutant, both the SG and GG point mutant caspase-9 significantly lost the ability to interact with and to be inhibited by BIR3 (Fig. 3d, middle and right panels). This observation indicates that the first two residues in the p12 subunit of caspase-9 are important for binding to BIR3 and inhibition.

As caspase-3 is not inhibited by BIR3 (concentration giving 50% inhibition, $IC_{50} > 400$ nM), we asked whether substitution of the first four residues of caspase-3-p12 with AVPF, which are the same residues present at the N-terminus of caspase-9-p12, could allow binding to and inhibition by BIR3. As shown in Fig. 3e, mutation of the first two residues of caspase-3 to AV allowed weak binding to XIAP and inhibition by BIR3 ($IC_{50} \approx 140$ nM). Mutation of the first four residues to AVPF enhanced binding to XIAP and increased inhibition by BIR3 ($IC_{50} \approx 4$ nM). These mutations also enhanced inhibition of caspase-3 by BIR2 of XIAP (IC_{50} values: WT, ~10 nM; AV, ~7 nM; AVPF, ~4 nM). This is consistent with the recent findings that BIR2 can also bind the AVPI peptide of Smac[7,11].

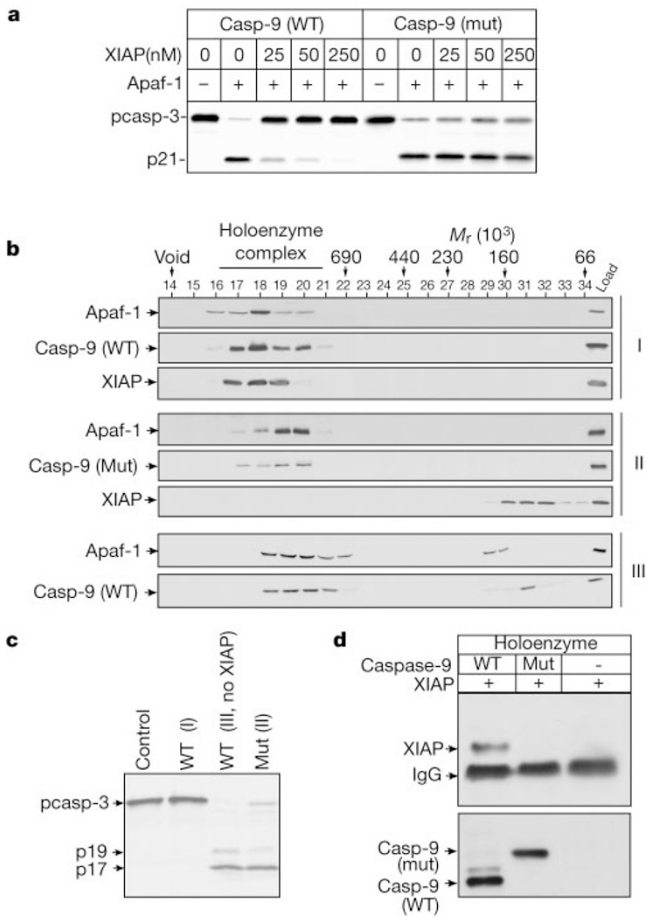

Figure 2 Proteolytic processing of caspase-9 is important for XIAP-inhibition. **a**, Autoradiographic analysis of processing of ^{35}S-labelled procaspase-3 by the fully processed WT, and the unprocessed triple-mutant caspase-9 holoenzyme complexes in the presence of different amounts of XIAP. **b**, Superose-6 gel filtration analysis of the WT or triple-mutant caspase-9 holoenzyme complexes reconstituted with XIAP (panels I and II) or nothing (panel III). The column fractions were analysed by western blotting with anti-Apaf-1, anti caspase-9 or anti-XIAP antibodies. **c**, Autoradiographic analysis of processing of ^{35}S-labelled procaspase-3 by the holoenzyme complexes from runs I (WT), III (WT, no XIAP) and II (Mut), respectively. Lane 1, buffer control. **d**, FPLC-purified holoenzyme complexes containing WT or triple-mutant caspase-9 were incubated with XIAP and then immunoprecipitated with anti-Apaf-1 antibody. The immunoprecipitates were analysed by western blotting with an XIAP antibody (upper panel) or a caspase-9 antibody (lower panel).

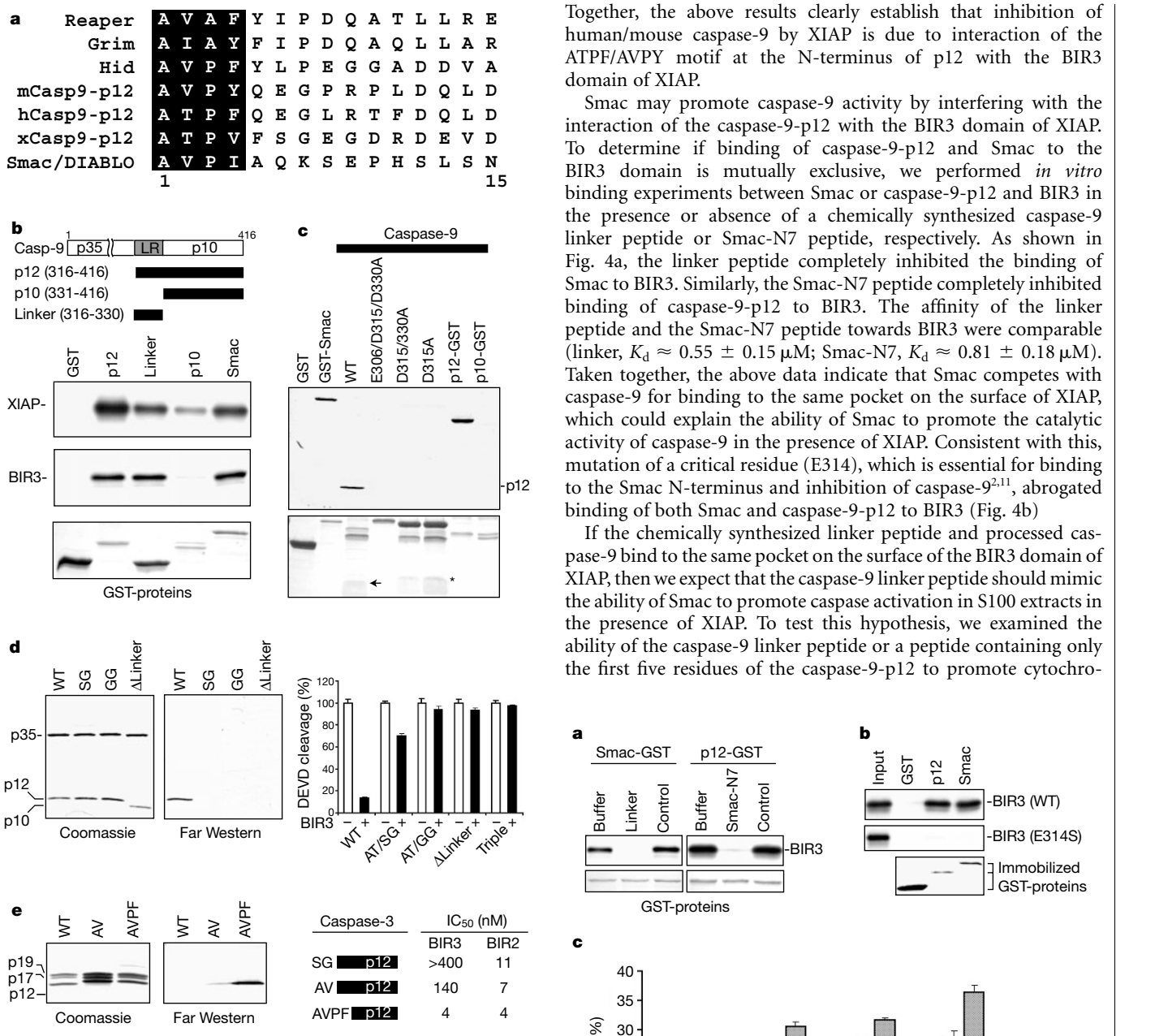

Figure 3 The N terminus of the p12 subunit of caspase-9 harbours a BIR3-binding motif. **a**, Collinear alignment of the N-terminal sequences of *Drosophila* Reaper, Grim and Hid, mouse, human and *Xenopus* caspase-9-p12, and human Smac. The BIR3-binding motif is highlighted. **b**, Autoradiographic analysis of the interactions of ^{35}S-labelled XIAP, or BIR3 domain of XIAP with C-terminal GST-tagged caspase-9-p12 (residues 316–416, p12), linker region (residues 316–330, linker) or p10 (residues 331–416, p10), or mature Smac (Smac). **c**, Upper panel, far-western blot analysis of recombinant WT or mutant caspase-9, or Smac-GST fusion protein with ^{35}S-labelled XIAP as described in Methods. Lower panel, Coomassie stained gel of all the indicated proteins. Arrow indicates p12 of caspase-9. Asterisk indicates p14 of caspase-9, which is generated by processing at E306. **d**, Equal amounts of recombinant WT or mutant caspase-9 (AT316, 317SG, AT316, 317GG and Δlinker) were fractionated by SDS-PAGE and Coomassie stained (left panel), or analysed by far western as in **c** (middle panel), or reconstituted with Apaf-1 and cytochrome *c* plus dATP in the presence (+) or absence (–) of purified XIAP-BIR3 (20 nM) in caspase-9–Apaf-1 deficient S100 extracts (right panel). The activity of each reconstituted extract is represented as % DEVD cleavage relative to the DEVD-AMC cleaving activity in the absence of BIR3. **e**, Recombinant WT or mutant caspase-3 (SG176, 177AV or SGVD176-179AVPF) were fractionated by SDS-PAGE and Coomassie stained (left panel) or analysed by far western as in **c** (middle panel). Right panel shows the calculated IC_{50} values for the WT (SG) and the indicated caspase-3 mutants as calculated from the percentage of inhibition by BIR3-RING (BIR3) or BIR1-BIR2 (BIR2) of XIAP.

Together, the above results clearly establish that inhibition of human/mouse caspase-9 by XIAP is due to interaction of the ATPF/AVPY motif at the N-terminus of p12 with the BIR3 domain of XIAP.

Smac may promote caspase-9 activity by interfering with the interaction of the caspase-9-p12 with the BIR3 domain of XIAP. To determine if binding of caspase-9-p12 and Smac to the BIR3 domain is mutually exclusive, we performed *in vitro* binding experiments between Smac or caspase-9-p12 and BIR3 in the presence or absence of a chemically synthesized caspase-9 linker peptide or Smac-N7 peptide, respectively. As shown in Fig. 4a, the linker peptide completely inhibited the binding of Smac to BIR3. Similarly, the Smac-N7 peptide completely inhibited binding of caspase-9-p12 to BIR3. The affinity of the linker peptide and the Smac-N7 peptide towards BIR3 were comparable (linker, $K_d \approx 0.55 \pm 0.15\,\mu M$; Smac-N7, $K_d \approx 0.81 \pm 0.18\,\mu M$). Taken together, the above data indicate that Smac competes with caspase-9 for binding to the same pocket on the surface of XIAP, which could explain the ability of Smac to promote the catalytic activity of caspase-9 in the presence of XIAP. Consistent with this, mutation of a critical residue (E314), which is essential for binding to the Smac N-terminus and inhibition of caspase-9[2,11], abrogated binding of both Smac and caspase-9-p12 to BIR3 (Fig. 4b)

If the chemically synthesized linker peptide and processed caspase-9 bind to the same pocket on the surface of the BIR3 domain of XIAP, then we expect that the caspase-9 linker peptide should mimic the ability of Smac to promote caspase activation in S100 extracts in the presence of XIAP. To test this hypothesis, we examined the ability of the caspase-9 linker peptide or a peptide containing only the first five residues of the caspase-9-p12 to promote cytochro-

Figure 4 Binding of caspase-9-p12 or Smac to the BIR3 domain is mutually exclusive. **a**, Autoradiographic analysis of the interactions of ^{35}S-labelled BIR3 with Smac-GST or p12-GST proteins in the absence (buffer) or presence of 200 μM linker peptide (Smac-GST, left panel) or Smac-N7 peptide (p12-GST, right panel) or non-specific peptide (control). **b**, Autoradiographic analysis of the interactions of ^{35}S-labelled WT BIR3 or E314S mutant BIR3 with GST, p12-GST, or Smac-GST proteins. **c**, 293T S100 extracts were mixed with purified XIAP (10 nM) and then stimulated with cytochrome *c* plus dATP in the presence of increasing amounts of a non-specific peptide (control), Smac-N5, p12-N5 or linker peptides (25, 100, 500 μM). The reactions were carried out in the presence of DEVD-AMC as a substrate. Control peptide, MKSDFYFQK, Smac-N5 peptide, AVPIA; p12-N5 peptide, ATPFQ; linker peptide, ATPFQEGLRTFDQLD.

me-*c*-dependent activation of caspase-3 in S100 extracts containing XIAP (Fig. 4c). The activity of caspase-3 in the S100 extracts was measured using the peptide substrate DEVD-AMC. Both the linker and the p12-N5 peptides were as effective in promoting caspase-3 activation as the Smac-N5 or N7 (not shown) peptides in the XIAP-containing extracts. These results confirm that the linker peptide can compete with caspase-9 for binding to BIR3 and could function as an inhibitor of XIAP. During apoptosis, caspase-9 is further processed at Asp 330 by the activated caspase-3[10,12]. On the basis of the above observations, processing at Asp 330 not only relieves the inhibition of caspase-9 by XIAP, but also releases the linker peptide into the cytoplasm, which could bind to XIAP and neutralize its inhibitory activity. Thus from a physiological aspect, the release of the linker peptide from caspase-9 during apoptosis constitutes a positive feedback loop in the potentiation of the caspase cascade and apoptosis.

Our observations reveal a mechanism for the activation and inhibition of caspase-9. Unlike other caspases, proteolytic processing of caspase-9 serves as a mechanism for inhibition, rather than activation. In the absence of proteolytic processing, XIAP is unable to interact with procaspase-9 or inhibit its enzymatic activity. Upon apoptotic stimuli, procaspase-9 undergoes auto-catalytic processing in the context of a holoenzyme that contains Apaf-1 and cytochrome *c*, in which the apoptosome serves as the allosteric regulator of the caspase-9 activity[10,12].

In the crystal structure of a Smac–XIAP complex, the N-terminal tetra-peptide of Smac binds a surface groove on the BIR3 domain of XIAP (Fig. 5a), making a network of hydrogen-bond interactions and extensive van der Waals contacts[13]. The side chain of the first residue Ala fits in a conserved hydrophobic pocket in the surface groove of XIAP, which is formed in part by Trp 310 (Fig. 5a). The Ala main-chain groups hydrogen-bond to surrounding XIAP residues, including a pair of charge-stabilized hydrogen bonds to Glu 314. The high sequence similarity between the N-terminal sequences of the p12 subunit of caspase-9 and Smac predicts an identical mode of interaction with the BIR3 domain of XIAP (Fig. 5a). This is indeed supported by our experimental observations (Figs 3 and 4). The first residue Ala of the tetra-peptide is partially embedded in a pocket and uses its fully exposed amino group to hydrogen-bond to Glu 314, explaining why procaspase-9 must be proteolytically processed before it can bind XIAP (Fig. 2). In agreement with this prediction, mutation of Trp 310 or Glu 314 resulted in abrogation or significant reduction of interactions with both Smac and caspase-9 (Fig. 4, and data not shown).

The physical binding of the N-terminus of the caspase-9 p12 subunit to the BIR3 domain of XIAP constitutes an indispensable step in the inhibition of caspase-9. The close proximity of the N-terminus of the p12 subunit and the catalytic residue of caspase-9 suggests that XIAP may hinder the entry of the substrate to the active site (Fig. 5b). This proposed model is further supported by the observation that mutation of His 343 in XIAP-BIR3 results in complete loss of inhibition to the enzymatic activity of caspase-9[2], but not binding to caspase-9-p12 (data not shown), suggesting that His 343 directly binds the active site of caspase-9. Thus, although binding of the tetra-peptide of caspase-9 by XIAP appears to be a major contributor in their mutual interaction, other weaker interactions between caspase-9 and XIAP also contribute to the inhibition of caspase-9. Furthermore, the IAP proteins are likely to dimerize in solution[7], which could further block substrate entry.

If Smac peptide interacts with the BIR3 domain of XIAP in the same manner as does caspase-9, how can Smac be more effective in relieving the inhibition of caspase-9? First, in addition to the tetra-peptide binding, Smac uses an extensive second interface to interact with the BIR3 domain of XIAP, involving over 2,000 Å^2 burial surface area[13]. This additional interaction may tip the balance in favour of the Smac–XIAP complex. Second, Smac also binds tightly to the BIR2 domain of XIAP[7], which could facilitate the Smac–BIR3 interactions. Third, cleavage of caspase-9 after Asp 330 releases the linker peptide, which further helps to remove the inhibition of caspase-9 by XIAP. Finally, in apoptotic cells, the amount of Smac released from the mitochondria could be in excess.

The activation of procaspase-9 represents a critical step in the mitochondria-initiated apoptotic pathways. However, XIAP is unable to bind and inhibit procaspase-9 but binds and inhibits the proteolytically processed mature caspase-9. More strikingly, the mature caspase-9 uses the same conserved tetra-peptide to interact with XIAP as the mature form of Smac. These conserved interactions lead to opposing effects in caspase-9 activity and consequently apoptosis. □

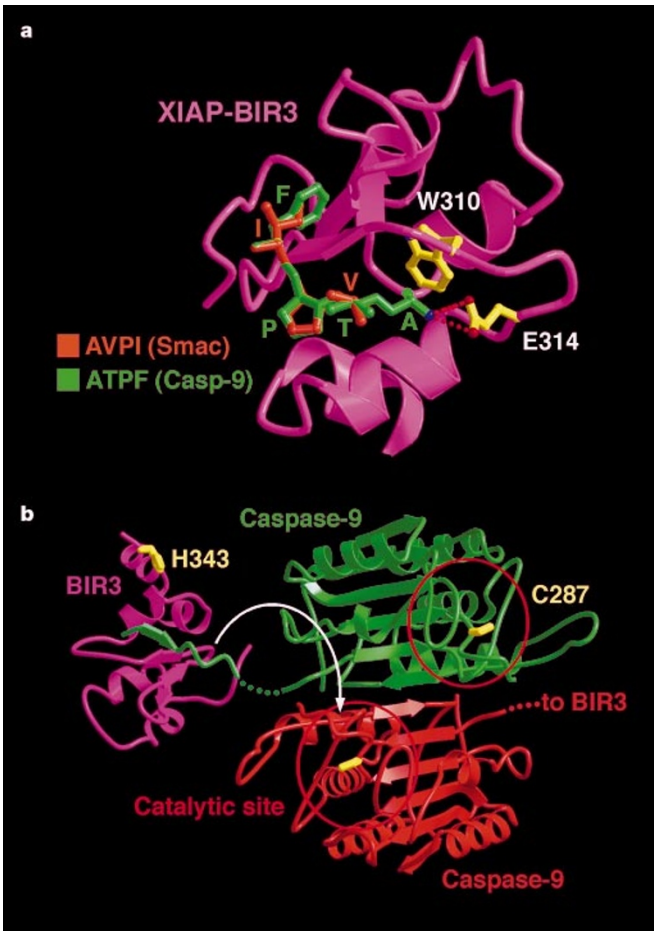

Figure 5 A proposed model of caspase-9 inhibition by XIAP. **a**, Conserved binding of BIR3 by caspase-9 and by Smac. XIAP-BIR3 is shown in pink. The N-terminal tetra-peptides from Smac (AVPI) and the p12 subunit of the human caspase-9 (ATPF) are shown in orange and green, respectively. Two critical residues on the BIR3 domain, W310 and E314, are highlighted in yellow. The N-terminal tetra-peptide (AVPY) from the p12 subunit of the rat or mouse caspase-9 more closely resembles the Smac peptide (AVPI). **b**, A proposed model of caspase-9 inhibition by XIAP. The dimer of mature caspase-9 (based on the atomic coordinates of caspase-3, PDB code 1DD1) is represented by green and orange whereas the BIR3 domain of XIAP is shown in pink. The approximate location of the catalytic residue on caspase-9, C287, is highlighted in yellow. The catalytic site is identified by a red circle. H343, which is implicated in binding the catalytic site of caspase-9 is also shown in yellow.

Methods

cDNA cloning and expression of recombinant proteins

All caspase-9, caspase-3 and their mutant counterparts were overexpressed in *Escherichia coli* strain BL21(DE3) as C-terminally 6-histidine-tagged proteins using pET-21c or pET-28a vector (Novagen). Full length XIAP and its BIR3-RING (residues 243–497) or BIR1-BIR2 (residues 1–242) domain were overexpressed in *E. coli* strain DH5α as N-terminally

GST-tagged proteins using a pGEX 4T vector (Pharmacia). Full-length XIAP, BIR3 and mutant BIR3 were *in vitro* translated in the presence of ^{35}S-methionine in reticulocyte lysates using MYC-pcDNA3 vector. Smac, caspase-9-p12, p10 and linker peptide were overexpressed in *E. coli* strain BL21(DE3) as C-terminally GST-tagged proteins using a pET-28-GST vector. Apaf-1L was expressed in Sf-9 insect cells and purified to homogeneity as previously described[14].

Reconstitution and assay of the activity of the caspase-9–Apaf-1 holoenzyme complexes

Recombinant WT and mutant caspase-9 proteins (20 nM) were incubated in the presence or absence of recombinant Apaf-1 (20 nM) in buffer A[6]. The reaction mixtures were stimulated with cytochrome *c* (5 ng μl^{-1}) and dATP (1 mM) and incubated for 0–60 min at 30 °C with purified procaspase-3 C163A, and the processing of procaspase-3 was analysed by western blot analysis with anti-caspase-3 antibody (Fig. 1c). The holoenzyme complexes were also reconstituted as above in caspase-9-depleted S100 extracts from Apaf-1-deficient mouse embryonic fibroblasts (Fig. 1d). The DEVD-AMC cleaving activity of the reconstituted extracts were measured over a time of 0–120 min by luminescence spectrometry and represented in arbitrary spectrometric units. In some experiments the WT and the unprocessed triple-mutant (E306/D315/330A) caspase-9 proteins (specific activity ~10 fluorogenic units per s per ng) were reconstituted with Apaf-1 and cytochrome *c* plus dATP in the presence of increasing amounts of XIAP, and the cleavage of ^{35}S-labelled procaspase-3 by the complexes was analysed by SDS-PAGE and autoradiography (Fig. 2a).

Gel-filtration analysis of the caspase-9–Apaf-1 holoenzyme complexes

These procedures were performed as described before[14]. Caspase-9–Apaf-1 holoenzyme complexes containing WT or mutant caspase-9 were reconstituted in the presence of cytochrome *c* (5 ng μl^{-1}) and dATP (1 mM) in oligomerization buffer I (25 mM HEPES (pH 7.4), 50 mM NaCl, 10 mM KCl, 5 mM MgCl2, 100 $\mu g\ ml^{-1}$ BSA, 5% glycerol, and 0.1 mM DTT) for 1 h at 30 °C. After incubation, the reaction mixtures were diluted with oligomerization buffer I and aliquots of each sample (100 μl) were loaded onto Superose-6 FPLC column. Equal volumes of the column fractions (50 μl) were separated by SDS-PAGE and immunoblotted with anti-Apaf-1 and anti caspase-9. In some experiments, the holoenzyme complexes were reconstituted in the presence of XIAP (Fig. 2b).

Far-western blotting

Affinity purified proteins were subjected to SDS-PAGE and were transferred to nitrocellulose membrane using standard western blotting techniques. The proteins on the membrane were denatured in a buffer (10 mM sodium phosphate pH 7.4, 150 mM sodium chloride, 5 mM magnesium chloride and 1 mM DTT) containing 6 M guanidine-HCl. The proteins were renatured by gradual reduction of guanidine-HCl to 0.3 M. The membrane was blocked overnight in the same buffer containing 5% non-fat dry milk and then incubated with ^{35}S-labelled *in vitro* translated XIAP in the same buffer with 1% non-fat dry milk. The membrane was washed at least three times and then exposed to X-ray film.

In vitro interaction assays

All *in vitro* interactions were performed as described[6].

Determination of IC_{50}

WT caspase-3 or caspase-3 mutant proteins (10 pM) were incubated with purified BIR3 (0.5–800 nM) or BIR1-BIR2 proteins (0.1–80 nM) at 37 °C in the presence of DEVD-AMC (100 μM) for 30 min and the substrate cleavage was measured by luminescence spectrometry. The IC_{50} values were then calculated using Graphpad Prism V2.0 (Graphpad Prism Software, San Diego, CA).

DEVD cleavage assays

Caspase-3 enzymatic assays with the tetrapeptide substrate DEVD-AMC were performed as described[6].

Computer modelling

On the basis of the crystal structure of a Smac–BIR3 complex[13], the N-terminal tetrapeptide of Smac was replaced by that from the p12 subunit of human caspase-9. Then we performed limited energy minimization on the complex between BIR3 and the tetrapeptide from the p12 subunit of the human caspase-9.

Received 4 December 2000; accepted 1 February 2001.

1. Deveraux, Q. L. *et al.* Cleavage of human inhibitor of apoptosis protein XIAP results in fragments with distinct specificities for caspases. *EMBO J.* **18,** 5242–5251 (1999).
2. Sun, C. *et al.* NMR structure and mutagenesis of the third BIR domain of the inhibitor of apoptosis protein XIAP. *J. Biol. Chem.* **275,** 33777–33781 (2000).
3. Datta, R. *et al.* XIAP regulates DNA damage-induced apoptosis downstream of caspase-9 cleavage. *J. Biol. Chem.* **275,** 31733–31738 (2000).
4. Verhagen, A. M. *et al.* Identification of DIABLO, a mammalian protein that promotes apoptosis by binding to and antagonizing IAP proteins. *Cell* **102,** 43–53 (2000).
5. Du, C., Fang, M., Li, Y., Li, L. & Wang, X. Smac, a mitochondrial protein that promotes cytochrome c–dependent caspase activation by eliminating IAP inhibition. *Cell* **102,** 33–42 (2000).
6. Srinivasula, S. M. *et al.* Molecular determinants of the caspase-promoting activity of Smac/DIABLO and its role in the death receptor pathway. *J. Biol. Chem.* **275,** 36152–36157 (2000).
7. Chai, J. *et al.* Structural and biochemical basis of apoptotic activation by Smac/DIABLO. *Nature* **406,** 855–862 (2000).
8. Abrams, J. M. An emerging blueprint for apoptosis in *Drosophila*. *Trends Cell. Biol.* **9,** 435–440 (1999).
9. Chen, P., Nordstrom, W., Gish, B. & Abrams, J. M. Grim, a novel cell death gene in *Drosophila*. *Genes Dev.* **10,** 1773–1782 (1996).
10. Srinivasula, S. M., Ahmad, M., Fernandes-Alnemri, T. & Alnemri, E. S. Autoactivation of procaspase-9 by Apaf-1-mediated oligomerization. *Mol. Cell* **1,** 949–957 (1998).
11. Liu, Z. *et al.* Structural basis for binding of Smac/DIABLO to the XIAP BIR3 domain. *Nature* **408,** 1004–1008 (2000).
12. Rodriguez, J. & Lazebnik, Y. Caspase-9 and APAF-1 form an active holoenzyme. *Genes Dev.* **13,** 3179–3184 (1999).
13. Wu, G. *et al.* Structural basis of IAP recognition by Smac/DIABLO. *Nature* **408,** 1008–1012 (2000).
14. Saleh, A., Srinivasula, S. M., Acharya, S., Fishel, R. & Alnemri, E. S. Cytochrome c and dATP-mediated oligomerization of Apaf-1 is a prerequisite for procaspase-9 activation. *J. Biol. Chem.* **274,** 17941–17945 (1999).

Acknowledgements

We thank R. Penn for help with calculating IC_{50} values. This work was supported by the NIH (E.S.A, P.D.R, Y.S.). S.M.S. is a special fellow of the Leukemia and Lymphoma Society; Y.S. is a Searle scholar and a Rita Allen scholar.

Correspondence and requests for materials should be addressed to E.S.A. (e-mail: : E_Alnemri@lac.jci.tju.edu).

Methylation of histone H3 lysine 9 creates a binding site for HP1 proteins

Monika Lachner*, Dónal O'Carroll*, Stephen Rea, Karl Mechtler & Thomas Jenuwein

Research Institute of Molecular Pathology (IMP), The Vienna Biocenter, Dr Bohrgasse 7, A-1030 Vienna, Austria
** These authors contributed equally to this work*

Distinct modifications of histone amino termini, such as acetylation, phosphorylation and methylation, have been proposed to underlie a chromatin-based regulatory mechanism[1,2] that modulates the accessibility of genetic information. In addition to histone modifications that facilitate gene activity, it is of similar importance to restrict inappropriate gene expression[3,4] if cellular and developmental programmes are to proceed unperturbed. Here we show that mammalian methyltransferases that selectively methylate histone H3 on lysine 9 (Suv39h HMTases)[5] generate a binding site for HP1 proteins—a family of heterochromatic adaptor molecules[6,7] implicated in both gene silencing and supra-nucleosomal chromatin structure. High-affinity *in vitro* recognition of a methylated histone H3 peptide by HP1 requires a functional chromo domain; thus, the HP1 chromo domain is a specific interaction motif for the methyl epitope on lysine 9 of histone H3. *In vivo*, heterochromatin association of HP1 proteins is lost in *Suv39h* double-null primary mouse fibroblasts but is restored after the re-introduction of a catalytically active SUV39H1 HMTase. Our data define a molecular mechanism through which the SUV39H–HP1 methylation system can contribute to the propagation of heterochromatic subdomains in native chromatin.

The 'histone code' hypothesis[1,2] predicts that distinct modifications of the histone N termini can regulate interaction affinities for chromatin-associated proteins, similar to the binding of transcription factors to specific DNA sequences. For example, the acetylation of histone H4 tails induces an increased affinity for bromo-domain proteins[8], thereby recruiting histone acetyltransferases (HATs) to nucleosomal regions of transcriptional activity. The human (SUV39H1) or murine (Suv39h1) histone